Assessment of engineering gas radiative property models in high pressure turbulent jet diffusion flames

Jean-Louis Consalvi, Frédéric André, F.R. Coelho, F.H.R. Franca, F. Nmira, M. Galtier, V. Solovjov, B.W. Webb

ASSESSMENT OF ENGINEERING GAS RADIATIVE PROPERTY MODELS IN HIGH PRESSURE TURBULENT JET DIFFUSION FLAMES

J.L. Consalvi[1], F. Andre[2*], F.R. Coelho[3], F.H.R. Franca[3], F. Nmira[4], M. Galtier[2], V. Solovjov[5], B.W. Webb[5]

[1]Aix-Marseille Université, IUSTI/ UMR CNRS 7343, 5 rue E. Fermi, 13453 Marseille, France.

[2]Univ Lyon, CNRS, INSA-Lyon, Université Claude Bernard Lyon 1, CETHIL UMR5008, F-69621 Villeurbanne, France.

[3] Department of Mechanical Engineering, Federal University of Rio Grande do Sul, Porto Alegre, RS, Brazil

[4]Direction R&D EDF, 6 quai Watier, 78400 Chatou, France.

[5]Brigham Young University, 360G EB, Provo, UT 84602, USA

[*] Corresponding author. Email: frederic.andre@insa-lyon.fr

ABSTRACT. This article aims to determine the most relevant engineering global method for gas radiative property modeling to be applied in the simulations of combustion problems. Two versions of the full-spectrum correlated k (FSCK) model, the Rank-Correlated full-spectrum *k*-distribution/ Spectral-Line-Weighted-sum-of-gray-gases (RC-FSK/RC-SLW) and a new version of the Weighted-Sum-of-Grey-Gases (WSGG) model are compared with the Narrow-Band CK (NBCK) model in four turbulent axisymmetric jet diffusion flames fueled either by hydrogen or methane at atmospheric and higher pressures. These comparisons are performed in decoupled radiative heat transfer calculations with the thermal fields being prescribed. The databases and coefficients associated to these different models are determined from a unique Line-By-Line database in order to allow a relevant comparison. Model results suggest that the SLW/FSCK methods coupled to the so-called improved scheme proposed by Cai and Modest or the Rank-Correlated SLW/FSK model, along with k-g distributions generated from accurate high-resolution high-temperature databases are the most mature gas radiative property models to be implemented in CFD codes dealing with combustion problems involving gas-soot mixtures.

1. INTRODUCTION

The modeling of turbulent combustion processes is a difficult task that involves complex unsteady reacting flows, chemical kinetic, pollutant production, radiative heat transfer, and all these processes are coupled with turbulence [1]. Although thermal radiation is an important part of these problems with its importance increasing in high pressure or oxygen-enriched environments [1], the computational cost related to its modeling has to remain reasonable to allow the use of state of the art sub-models for the other processes.

This has motivated the development of new engineering gas radiative property models over the last two decades such as the SLW model [2], the FSCK model [3] and the SLMB model [4], or the improvement of already existing models such as the WSGG [5]. Despite differences in formulation, developments, refinements, and implementation, SLW and FSCK methods are based on the same reordering concept of the absorption coefficient, provide rigorously Line-by-Line accuracy for uniform media and can be easily implemented in CFD codes owing to the development of databases or correlations and mixing methods to treat gas-soot mixtures [6-10]. In the case of non-uniform media, both methods introduce the assumption of correlated *k*-distribution and different schemes were developed to get the local absorption coefficient in such situations [2, 3, 11]. These schemes require, in general, the definition of a reference thermodynamic state. Recently, the assumption of Rank Correlated (RC) / comonotonic [12] spectrum was introduced, leading to either the RC-SLW model [13] or the RC-FSK model [14], which were found to be identical when the same strategy is applied to evaluate the gray gases weights [14]. The Rank Correlated method requires no specification of a reference gas thermodynamic state. The RC-SLW method was recently assessed against state-of-the-art modeling approaches in Ref. [15] and was found to provide a high accuracy at a reasonable computational cost. In the same reference, the narrow band ℓ-distribution approach [16, 17] was found to yield a higher accuracy than the NBCK method, at a lower computational cost. However, the ℓ-distribution method cannot be used together with a RTE solver based on the DOM or Finite Volume

Method, as considered in the present work, which explains why the NBCK model is chosen here as a reference (see section 2.1).

The global objective of this study is to evaluate the capability of FSK, RC-SLW/RC-FSK and WSGG gas radiative property model to predict the radiative outputs in atmospheric and high pressure axisymmetric turbulent flames covering a wide range of optical-thicknesses and fuel sooting propensities. Previous studies showed that classical FSCK and SLW provide comparable solutions [18, 19] when used with similar conditions and only the FSCK formulation will be considered in the present paper. As a first step, this work reports decoupled radiative calculations with specified thermal fields.

2. GAS PROPERTY MODELS

This subsection presents the gas property models used in the present study. For each model, absorption spectra are required to generate the corresponding databases or model coefficients. In this study, the detailed spectral absorption cross-section database generated by Pearson [20] from HITEMP 2010 is used for all the models. This database covers the entire spectrum (0-25,000 cm^{-1}) with a resolution of 0.005 cm^{-1} for CO_2, H_2O and CO, for pressures and temperatures ranging from 0.1 to 50 atm and from 300 to 3000 K, respectively.

In a similar search of fairness among the different models, the soot absorption coefficient is computed for all the models from the Rayleigh theory coupled to the correlations of Ref. [21] for the refractive and absorptive indexes.

2.1 Narrow-band (NB) CK distribution models

Narrow-band database

A database of narrow band (NB) *k*-distributions for CO_2 and H_2O was generated from the LBL spectral absorption cross-section database of Pearson [20]. For each pressure of interest and radiating species, the NB *k-g* distributions were stored in the database for 128 values of *g* corresponding to a

128-point Gauss quadrature scheme, 9 mole fractions, x, ranging between 0 and 1 (0, 0.05, 0.1, 0.2, 0.3, 0.4, 0.6, 0.8, 1), 28 temperatures, T, ranging from 300 to 3000 K (by a uniform step of 100 K), and 998 narrow bands with a resolution of 25 cm^{-1}. LBL derived-NB database were found to predict radiative outputs within about 1% of direct LBL calculations in high-pressure flame calculations [19].

Reference solution

The reference solutions were obtained with the databases described above. At each computational grid node, the following procedure was used to determine the absorption coefficient used to solve the NB RTE from the narrow band database. For each species, the narrow band *k-g* distribution for each narrow band and each of the 128 Gauss points was interpolated from the database with linear interpolations on x and spline interpolations on T [6]. For each narrow band, a mixed NB k_m-g_m distribution was then obtained by using the mixing scheme of Modest and Riazzi [6]. For each narrow band, the absorption coefficients at the 10 Gauss points was used to solve the NB RTE are then obtained from the k_m-g_m distribution by using a linear interpolation.

Mixed NBCK

The NBCK model used to compute the reference solutions is too time consuming to be considered in coupled calculations. A simplified NB database was therefore generated from the NB database described above. First of all, the number of narrow bands is considerably reduced from 998 to 115 by using the lumping strategy described in Ref. [19]. Special attention was paid in the splitting of the spectrum to minimize the variation of the blackbody intensity over a low resolution narrow band. This reduced NB database considers mixed NB *k-g* tables using the mixing scheme of Modest and Riazzi [6]. For each lumped narrow band, the absorption coefficients of CO_2-H_2O mixtures of known mole fractions (CO is not considered in the present work) are stored in the database at the 10-Gauss points used to solve the NB RTE. At each computational grid node and for each NB and quadrature point, the absorption coefficient required to solve the NB RTE is extracted from the database by using

linear interpolations on x_{CO_2} and x_{H_2O} and a spline interpolation on *T*. This method will be referred to as Mixed NBCK hereafter.

2.2 FSCK methods

Full-Spectrum database. A full spectrum (FS) database was generated from the NB database described in the previous subsection. For each pressure of interest, mixed FS *k-g* pairs were stored in the database for 32 values of *g* corresponding to a 32-point Gauss quadrature scheme, 9 mole fractions ranging between 0 and 1 (0, 0.05, 0.1, 0.2, 0.3, 0.4, 0.6, 0.8, 1) for x_{CO_2} and x_{H_2O}, 6 values of the soot volume fractions, f_s, between 0 and 10^{-5} (0, 0.5×10^{-6}, 1.0×10^{-6}, 1.5×10^{-6}, 2.0×10^{-6}, 1.0×10^{-5}), 28 temperatures *T* ranging from 300 to 3000 K (by a uniform step of 100 K), and 28 values of the Planck-function temperature, T_P, (between 300 and 3000 K at an interval of 100 K). As discussed by Wang et al. [8], k-g distributions have a non-linear dependency with respect to the species mole fractions due to mixing and self-broadening. In particular, the non-linear effects due to mixing appear at low mole fractions. As a consequence, the non-uniform discretization of the mole fractions, optimized by Pearson and co-workers [9], [20], was adopted in the present study.

For each specific value of $\phi = \left\{ x_{CO_2}, x_{H_2O}, f_s, T \right\}$ and T_P, FS *k-g* tables were assembled from the following procedure: i) NB *k-g* values are mixed by using the mixing procedure of Modest and Riazzi [6], ii) within a NB, the absorption coefficient of a soot changes slowly with wavelength and thus, the absorption of particles can be simply treated as an addition to the NB cumulative *k-g* distribution. This is achieved by determining the average particle absorption coefficient across the narrow band and then adding it to the mixed NB reordered absorption coefficients, and iii) finally the mixed FS *k-g* values are assembled from the previously computed mixed NB *k-g* sets following the procedure of Modest and Riazzi [6]. For each FSCK simulation described below, the required *k-g* values at a given computational point are interpolated from the database by using linear interpolations on x_{CO_2}, x_{H_2O}, and f_s and spline interpolations on T and T_P.

More formally, the FS cumulative distribution function of a mixture of CO_2, H_2O and soot at some specified value k_{mix} of the mixture is evaluated by the following two-step process:

1/ For all narrow bands $\Delta\eta$, and for all mole fractions of CO_2, H_2O, volume fraction of soot particles and gas temperature, a cumulative distribution function for the mixture is first calculated as

$$\begin{aligned} g^{\Delta\eta}\left(k_{mix},\phi\right) &= \int_0^1\int_0^1 H\left[k_{mix} - x_{CO_2}k_{CO_2}\left(g_1\right) - x_{H_2O}k_{H_2O}\left(g_2\right) - k_{soot}\right] dg_1\, dg_2 \\ &\approx \sum_{i=1}^{N}\sum_{j=1}^{N} w_i \cdot w_j \cdot H\left[k_{mix} - x_{CO_2}k_{CO_2}\left(x_i\right) - x_{H_2O}k_{H_2O}\left(x_j\right) - k_{soot}\right] \end{aligned} \tag{1}$$

Here, weights and nodes of the Gauss-Legendre quadrature for the *k*-distribution model with 128 *k*-values are written as $w_i,\ i=1,..,N=128$ and $k_{\text{molecule}}\left(x_i\right),\ i=1,..,N=128$ respectively, and H is the Heaviside step function.

2/ The full spectrum distribution function is then obtained as the average over all narrow bands:

$$g\left(k_{mix},\phi,T_P\right) = \sum_{\text{all }\Delta\eta} \frac{I_{b,\eta}\left(T_P\right)}{I_b\left(T_P\right)} \cdot g^{\Delta\eta}\left(k_{mix},\phi\right) \tag{2}$$

Once this function is known, it can be used: 1/ to generate gray absorption coefficients of the gas-soot mixture at any local state, and 2/ the corresponding weights. Different models use different approaches to generate these coefficients from the same values of the cumulative distribution function. As soon as a method is chosen, it can be used to construct a look-up table (here, based on a discretization of the range of *k*-values into 32 gray gases plus soot) which can then be interpolated to estimate gas-soot radiative properties at any local state. This method is recommended when considering radiative heat transfer problems that involve many cells (In one-dimensional cases a direct evaluation of gray absorption coefficients and weights can be used).

FSCK Model. The full spectrum RTE is expressed as [3]:

$$\frac{dI_{g_0}}{ds} + k^*(g_0)I_{g_0} = k^*(g_0)a(g_0)I_b(T) \tag{3}$$

where g_0 corresponds in the present study to a quadrature-point of a 16-point Gauss-Chebyshev quadrature scheme, the index 0 referring to the reference state. The reference state is defined here by values of x_{CO_2}, x_{H_2O}, and f_s averaged over the flame volume defined by the isotherm 500 K. The reference temperature is calculated as the blackbody emission-averaged temperature [3].

The stretching factor, $a(g_0)$, is defined by Modest as [3]:

$$a(g_0) = \frac{dg(k_0,\phi_0,T)}{dg_0(k_0,\phi_0,T_0)} \tag{4}$$

Two schemes based on the assumption of correlated *k*-distribution were developed by Modest and co-workers to determine the absorption coefficient, $k^*(g_0)$, in Eq. (3):

1) The first scheme [3], referred to as the FSCK model hereafter, consists in solving $g(k^*,\phi,T_0) = g_0$ to get $k^*(g_0)$. However, this scheme does not preserve the total emission in practical applications due to the lack of linear relationship between the *k*-distributions. This scheme requires two *k*-distributions at each computational grid, $g(k,\phi,T_0)$ and $g(k_0,\phi_0,T)$, to determine the stretching factor.

2) The second scheme (termed the Improved FSCK scheme) [11], referred to as FSCK II hereafter, was developed to preserve the total emission. It consists in three steps: *i*) determine k_0 from $g(k_0,\phi_0,T_0) = g_0$, *ii*) interpolate the local value of $g = g(k_0,\phi_0,T)$, and *iii*) determine k^* from $g(k^*,\phi,T) = g(k_0,\phi_0,T)$. This scheme requires three *k*-distributions at each computational grid point, $g(k_0,\phi_0,T)$, $g(k,\phi,T)$ and $g(k_0,\phi_0,T)$.

Rank-Correlated (RC) FSK/SLW Model. The concept of Rank-Correlated spectrum was first developed for SLW methods [13] before being applied to the FSK methods [14]. The two approaches (Rank Correlated SLW and Rank Correlated FSK) were found to be theoretically identical, and

produce identical predictions when implemented using the same strategy to evaluate the gray gases weights [14]. The main advantage of the RC-FSK/SLW model is that no reference state is needed to make calculations in non-uniform media. A 16-point Gauss-Chebyshev quadrature scheme is also used for the RC-FSK model. The method consists in solving $g\left(k^*, \phi, T_p\right) = g_0$ in order to get k^* and to compute $g(k^*, \phi, T)$ to determine the stretching factor defined as:

$$a(g_0) = \frac{\partial g[k(g_0, \phi, T_p), \phi, T]}{\partial g_0} \tag{5}$$

Although T_p can be selected arbitrarily, it is taken equal as T_0 in the present study to be consistent with the other correlated FSK methods. However, it should be pointed out that this choice is different from that recommended by the developers of the Rank Correlated SLW method, who usually use a volume-averaged temperature. The sensitivity of the predictions to the choice of T_P in the RC-FSK/SLW method will be investigated hereafter as part of this study.

2.3 WSGG Model

The WSGG RTE can be written as [5]:

$$\frac{dI_j}{ds} + \kappa_j I_j = \kappa_j a_j I_b(T); 0 \leq j \leq J \tag{6}$$

where J is the total number of gray gases and the gray gas corresponding to j = 0 represents the transparent windows. The non-constant ratio WSGG model of Ref. [5] is considered here. In this model, the weighting factor for the j^{th} gray gas is given as $a_j = \sum_{k=1}^{K} b_{j,k}\, T^{k-1}$ where $b_{j,k}$ are polynomial coefficients and a_0 is computed as $a_0 = 1 - \sum_{j=1}^{J} a_j$ to ensure radiative energy conservation.

Two methods were considered to deal with arbitrary mixtures composed of CO_2, H_2O and soot. In the first, referred to as WSGGSP, the coefficients for the gas mixture were obtained from the coefficients for the individual species, assuming that the gray gas absorption coefficients are statistically independent [5]:

$$\kappa_j = x_{CO2} \times p \times \kappa_{pCO2,jc} + x_{H2O} \times p \times \kappa_{pH2O,jw} + f_S \times \kappa_{pS,jS};\ 0 \le j_w \le J_W, 0 \le j_c \le J_c, 1 \le j_S \le J_S \quad (7)$$

$$a_j = a_{CO2,j_c} \times a_{H2O,j_w} \times a_{S,j_S}; 0 \le j_w \le J_W, 0 \le j_c \le J_c, 1 \le j_S \le J_S \quad (8)$$

The total number of gray gases (and hence, the number of RTE to be solved) in the WSGGSP model is $J = (J_c + 1) \times (J_w + 1) \times J_S$ with $J_c = J_w = J_S = 4$.

In the second approach [22], the ratio x_{H_2O}/x_{CO_2} is assumed to be fixed and equal to 2 consistent with the complete combustion of methane in air, and the multiplication scheme (Eqs. 7 and 8) is applied to determine the WSGG parameters for the gas/soot mixture. The WSGG parameters for the H_2O/CO_2 mixtures were also generated based on the database of Pearson [20], using a similar methodology to the one from [23]. The number of RTEs to solve is then reduced by a factor of 5 as compared to the WSGGSP approach with $J = (J_{cw} + 1) \times J_S$ with $J_{cw} = J_S = 4$. This method will be referred to as the WSGGFR hereafter.

3. TEST CASES

3.1 Flame design

Two different combustion scenarios, turbulent co-flow H_2-air and CH_4-air jet diffusion flames, are considered in the present study. Two total pressures of 1 and 30 atm and 1 and 4 atm are considered for the H_2 and CH_4 flames, respectively, in order to increase the optical-thickness, and the fuel sooting propensity for the CH_4 flames. The injection conditions are summarized in Table 1. Following the

strategy developed in Ref. [24], the high-pressure flames were designed from the corresponding atmospheric cases based on Froude modeling. This allows the preservation of the flame geometry and the residence time as the pressure is scaled up.

Table 1. Operating conditions. U_F, U_{ox} and D_F represent the fuel injection velocity, the oxidizer injection velocity and the nozzle diameter, respectively. The penultimate and ultimate columns in Table 1 show the reference and flame peak temperatures, respectively.

Fuel	P (atm)	U_F ($m.s^{-1}$)	U_{ox} ($m.s^{-1}$)	D_F (mm)	$\dot{Q}_{abs}/\dot{Q}_{em}$ (-)	$\dot{Q}_{em,S}/\dot{Q}_{em}$ (-)	T_0 or T_P (K)	T_{peak} (K)
H_2	1	296.00	1.00	3.75	0.20	0	1263	2280
	30	296	1.00	3.75	0.69	0	1305	2310
CH_4	1	130.00	1.00	2.50	0.36	0.013	1257	1958
	4	130.00	1.00	2.50	0.50	0.33	1651	1917

3.2 Numerical model and methods

The turbulent jet diffusion flames are modelled using the computational model described in detail in Ref. [25]. It is based on a hybrid flamelet/transported composition PDF. The one point, one time joint composition PDF of the mixture fraction, enthalpy defect and representative soot properties is solved by using a Stochastic Eulerian Field (SEF) method developed by Valiño [26]. The flamelet libraries were generated using the full chemical kinetic scheme of Burke et al. [27] for the H_2 flames and Qin et al. [28] for the CH_4 flames. Soot production is modelled by a semi-empirical acetylene/benzene-based soot model [29]. Spectral gas and soot radiation is modelled using the mixed NBCK described previously. Absorption turbulence-radiation interactions (TRIs) are accounted for by using the Optically Thin Fluctuation Approximation (OTFA), and emission TRI is modelled 'exactly' by using a joint composition PDF.

3.3 Flame structure

Figure 1 shows the predicted fields of H_2O mole fraction (left side) and temperature (right side) for the H_2-air flame at atmospheric pressure. These fields are not shown for 30 atm since they are similar to those at 1 atm owing to the Froude modeling.

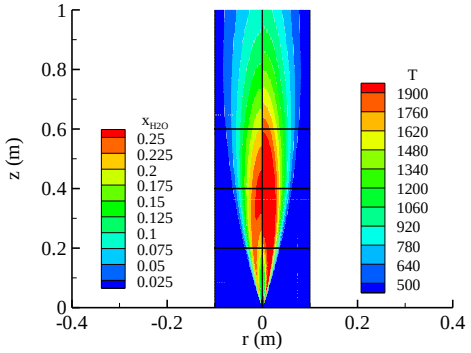

Figure 1. Fields of H_2O mole fraction (left) and temperature (right) for the H_2-air flame at 1 atm.

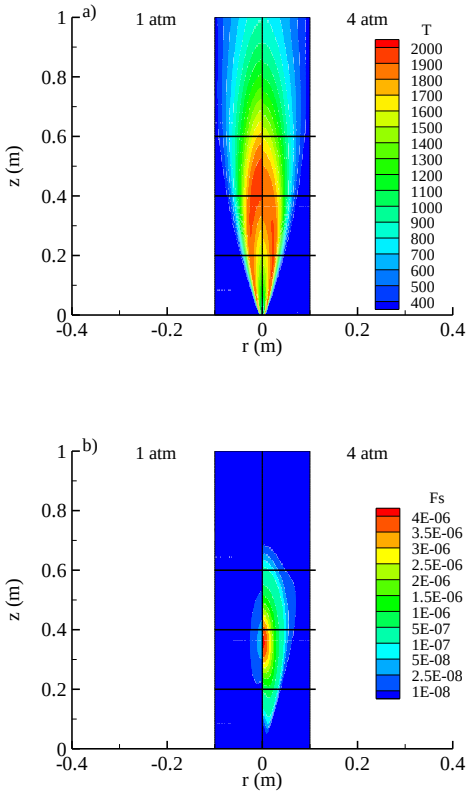

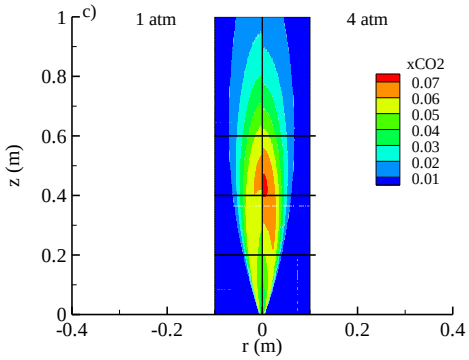

Figure 2. Fields of: a) temperature, b) soot volume fraction and c) CO_2 mole fraction for the CH_4 flames.

Figure 2 shows the fields of temperature, soot volume fraction and CO_2 mole fraction for the CH_4 flames. The soot production increases significantly as the pressure is scaled up from 1 to 4 atm with the peak soot volume fraction f_s increasing from about 0.03 ppm to 4.15 ppm (see Fig. 2b). This explains why the temperatures are, on the whole, lower at 4 atm than at 1 atm and the flame height is slightly lower. The horizontal lines in Figs. 1 and 2 represent the flame height locations z = 0.2 m, z = 0.4 m and z = 0.6 m where the capability of the different methods to predict the radiative source term will be investigated. These three locations are in the lower part of the flame, close to the middle of the flame and near the flame tip, respectively (see Figs. 1 and 2). In addition, Fig. 2b shows that, in the case of the sooting CH_4 flames, they correspond to regions where soot growth, reaches a maximum and are oxidized, respectively.

The sixth column in Table 1 represents the ratio between total absorption and total emission which characterizes the flame self-absorption and, in turn, the flame optical-thickness. As expected, the H_2-air flame at 1 atm is the thinnest flame, followed in the order of increasing optical-thickness by the 1-atm CH_4-air, the 4-atm CH_4-air flame and the 30-atm H_2-air flames. The seventh column of Table 1 represents the ratio of the emission due to soot to the total emission, thus quantifying the contribution of soot. The table reveals that soot contributes to about 1% of the emission in the 1-atm CH_4/air flame, showing that this flame can be considered as non-luminous. On the other hand, soot contributes about one-third of the total emission in the 4 atm CH_4/air flame.

4. RESULTS AND DISCUSSION

4.1 Metrics for the evaluation of the models

For all the gas spectral property models investigated here, the RTE is solved in axisymmetric configuration using the Finite Volume Method [30] employing an angular mesh with 12×16 control angles. It was checked that refining further the angular mesh does not affect the prediction of the radiative outputs. Relative errors on the radiative source term along radial profiles at specific heights of z = 0.2, 0.4, and 0.6 m and on the vertical profile of incident heat flux at a radial distance of r= 0.1 m from the flame axis will serve as metrics to compare the different models. The relative error for a computed variable ϕ is defined as:

$$Error = \frac{(|\phi_{model} - \phi_{reference}|)}{max(|\phi_{reference}|)} \tag{9}$$

The maximum value along the profile under consideration will be used in the denominator of Eq. (9).

4.2 Comparison of the different models

Figures 3 and 4 show the relative error in the radiative source term for the H_2 and the CH_4 flames, respectively. The mean and maximum relative errors are summarized in Table 2, whereas Table 3 reports the CPU times of the different methods and the two fuels considered in the present study. Mixed NBCK and FSCK models use pre-tabulated databases of mixed k-g distributions and, consequently, the CPU times related to these methods are affected neither by the pressure nor by the mixing process. The CPU times for these methods are slightly smaller for the CH_4 flames than for the H_2 flames owing to the lower number of cells used in the simulations (See Table3). In a similar way, the WSGG models use precomputed parameters and the corresponding CPU times also do not depend on pressure.

The mixed NBCK produces solutions in very close agreement with the reference solution and can therefore be used as reference in coupled calculations. It should be pointed out that the mixed NBCK is about 60 times faster than the reference.

Among the WSGG models existing in the literature, only the results of the WSGGSP model are reported in Figs. 3 and 4 in order to not overload them. The WSGGSP model is seen to yield predictions in good agreement with the reference with maximum and mean relative deviations being on the whole within 10% and 5% of the reference solutions, respectively. It can be observed in Table 2 that, for the 'non-luminous' flames (i.e., the H_2 flames and the CH_4 flame at 1 atm), the discrepancies generally increase with increasing optical thickness. Table 3 shows that the WSGGSP model is faster by a factor of 7-8 than the FSCK methods for the H_2 flames. For the CH_4 flames, the WSGGSP model requires the solution of 100 RTEs as compared to 16 RTEs for the FSCK methods. Consequently, the WSGG model becomes less computationally efficient than the FSCK methods. Table 2 shows that the accuracy of the WSGGFR model is also satisfactory for engineering combustion applications, which is in line with the conclusions drawn in Ref. [22]. These results suggest that WSGG parameters derived for equilibrium composition between CO_2 and H_2O can be applied for computing flame radiation. As discussed previously, the WSGGFR model improves considerably the computational efficiency of the WSGGSP model since only 20 RTEs must be solved instead (see Table 3). However, this remains larger than the number of RTEs to be solved for the FSCK-based radiation models.

The classical FSCK model also provides accurate engineering predictions although it is, on the whole, less accurate than the WSGG model. The FSCK scheme is very sensitive to the reference temperature, and predictions can be significantly improved by selecting a higher-temperature isotherm to determine the flame contour. In the present simulations, the reference temperature is significantly lower than the temperature as observed in the penultimate and last columns of Table 1. However, calibrating a reference temperature in coupled calculations is a delicate issue because the flame structure is not known á priori. The largest discrepancies are observed for the H_2/air flame at 1 atm

owing to its low optical thickness, which highlights the lack of accuracy of the FSCK scheme in the prediction of emission. The FSCK II and the RC-FSK models show substantial improvement in accuracy relative to the classical FSCK model, and provide solutions in very good agreement with the reference solution. For all the cases, these two methods (FSCK II and RC-FSK) generally predict radiative source term and heat flux within 5% of the reference. The shaded cells in Table 2 highlight the method that provides the best accuracy for each case. The FSCK II model appears to be the most accurate in some case whereas the RC-FSK model is the best for the other cases. However, the differences in error for the two models is slight. Therefore, these results do not allow the identification of the best method between the FSCK II and the RC-FSK models. Table 3 shows that the RC-FSK model is slightly more efficient from the computational point of view. However, it should be pointed out that the computational efficiency of the FSCK II scheme was considerably improved by the development of a new look-up table [31] and this new storage has not been considered in the present study. It should be further noted that the computation of the RC-FSK model may also be accelerated using several approaches, as suggested in [32, 33].

Table 2. Mean /maximum relative errors in percent for the different models. The errors for the radiative source term are based on the three radial profiles at z = 0.2, 0.4 and 0.6 m. The shaded cells highlight the most accurate method among the FSCK, FSCK II, RC-FSK and WSGG models. The selection of the most accurate model is based on both mean and max error.

Model/Flame		Mixed NBCK	FSCK	FSCK II	RC-FSK	WSGGSP	WSGGFR
H_2 1 atm	$-\nabla \cdot \dot{q}_R''$	0.36/0.64	7.66/20.20	0.72/2.36	1.50/3.45	2.36/4.21	-
	$\dot{q}_{R,w}''$	0.32/0.51	4.64/9.98	0.37/0.77	0.72/1.31	4.38/7.48	-
H_2 30 atm	$-\nabla \cdot \dot{q}_R''$	0.07/0.16	6.29/14.95	0.39/1.04	1.22/3.43	6.63/14.5	-
	$\dot{q}_{R,w}''$	0.19/0.34	4.46/9.61	4.04/6.45	1.79/4.13	4.13/8.26	-
CH_4 1 atm	$-\nabla \cdot \dot{q}_R''$	0.08/0.22	3.46/8.00	1.26/3.60	1.46/3.01	3.07/9.94	5.12/8.65
	$\dot{q}_{R,w}''$	0.10/0.20	1.70/3.68	0.76/1.57	1.66/2.62	4.32/7.11	5.04/12.2

CH_4 4 atm	$-\nabla \cdot \dot{q}_R''$	0.09/0.22	3.74/9.64	2.46/6.08	1.91/5.64	3.71/8.41	2.92/6.78
	$\dot{q}_{R,w}''$	0.04/0.09	2.04/5.12	0.96/2.32	1.09/1.78	0.71/1.51	0.53/1.11

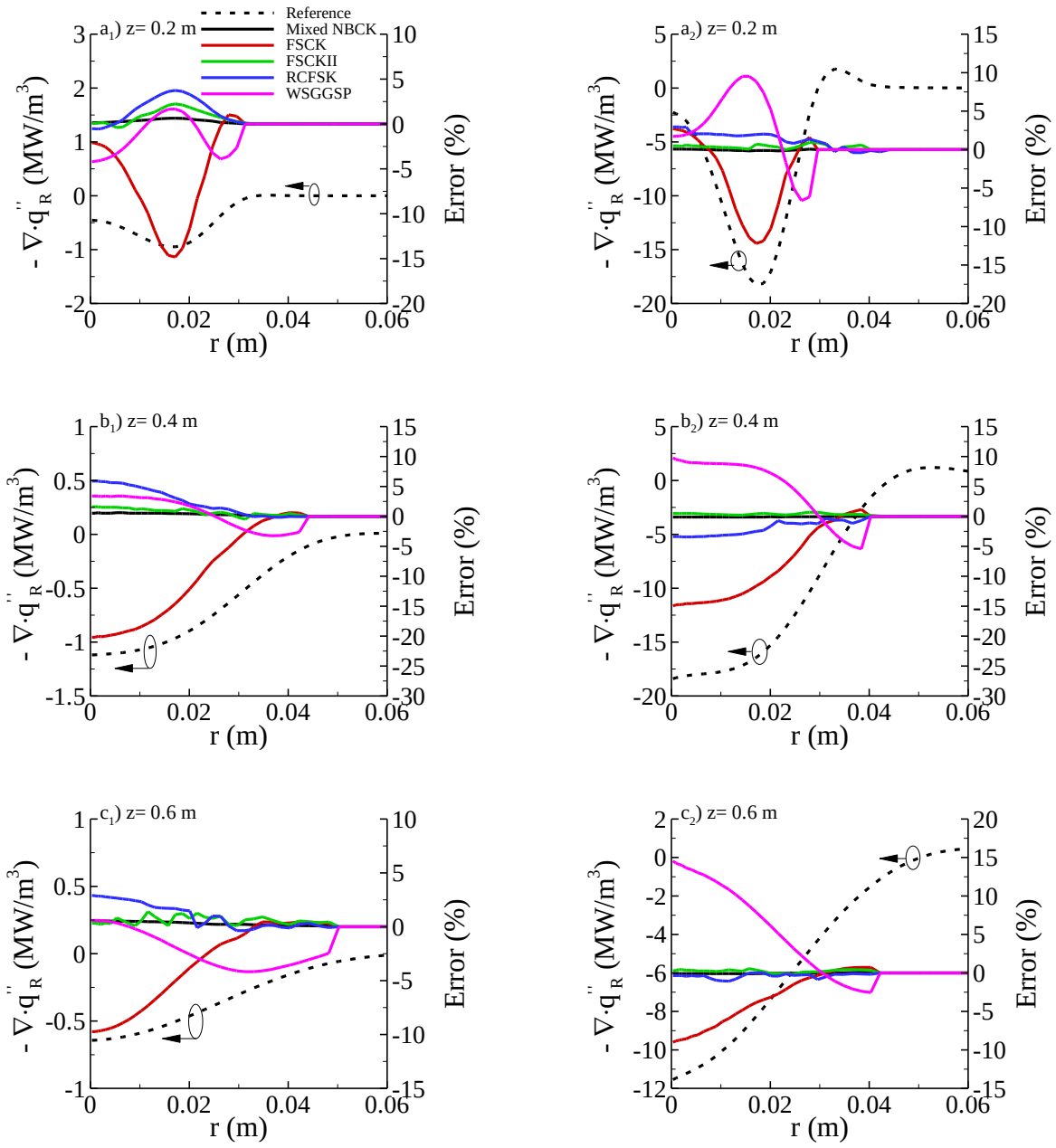

Figure 3. Radiative source term and relative error in percent as a function of the radial distance at different heights of: a) 0.2 m, b) 0.4 m and c) 0.6 m. The indexes 1 and 2 refer to the H_2/air flame at 1 atm and 30 atm, respectively.

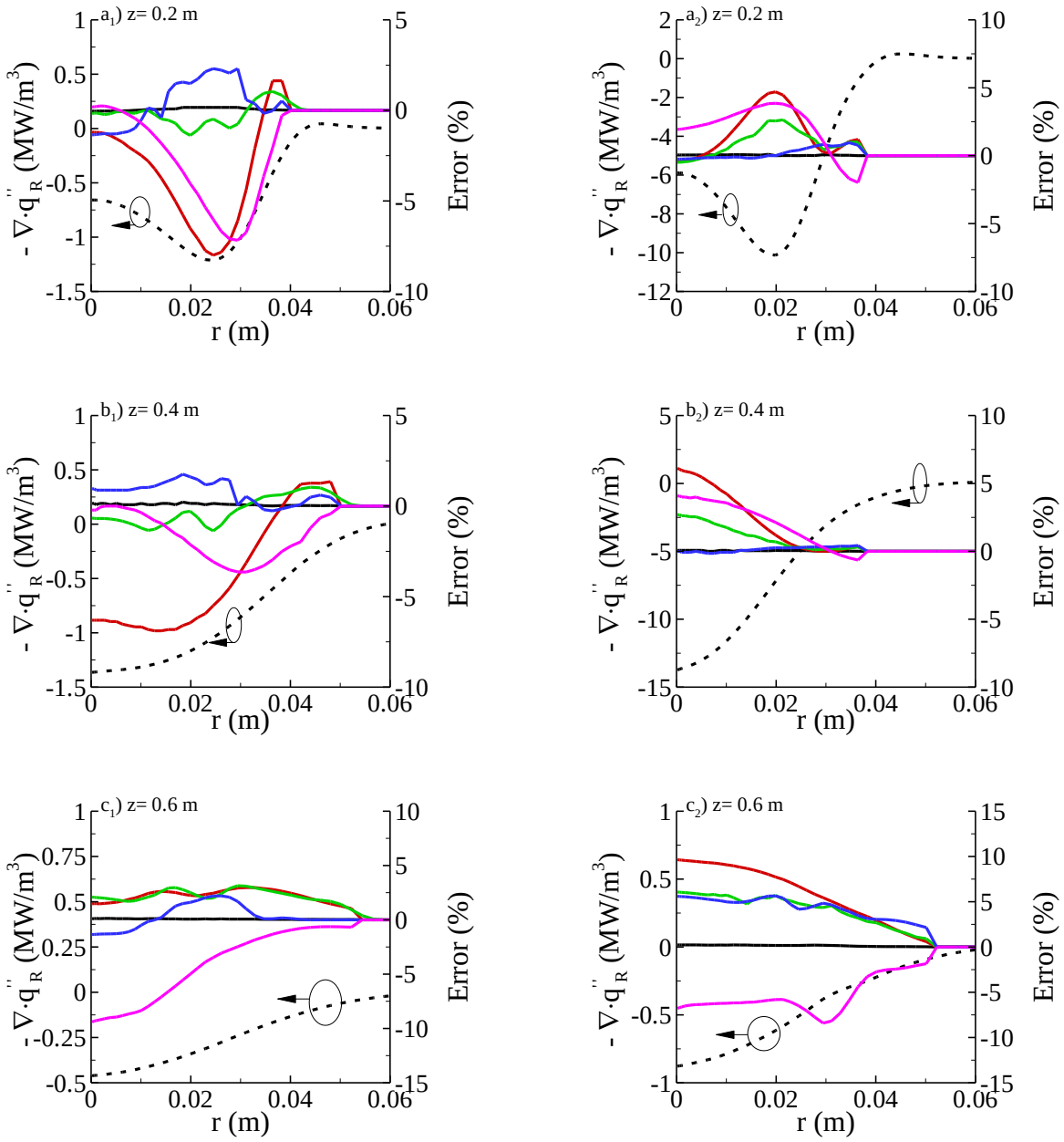

Figure 4. Radiative source term and relative error in percent as a function of the radial distance at different heights of: a) 0.2 m, b) 0.4 m and c) 0.6 m. The indexes 1 and 2 refer to the CH_4/air flame at 1 atm and 4 atm, respectively. See the legend of Fig. 3.

Table 3. CPU time (s) for the different models. The CPU times are for the complete radiation calculation including the spectral model and the RTE solver. The last column represents the number of cells. A 64-bit 2.9 GHz Intel Core i7-4910MQ CPU was used for the simulations.

Model/Flame	Mixed NBCK	FSCK	FSCK II	RC-FSK	WSGGSP	WSGGFR	Nber of cells
H_2	24	0.50	0.60	0.51	0.07	-	4590
CH_4	20	0.44	0.56	0.48	1.02	0.23	5022

3.3 Sensitivity of the FCSK II and RC-FSK models to reference/Planck temperature

The sensitivity of the FSCK II and RC-FSK models to the reference or Planck temperature, respectively, will be analyzed by considering the two methane flames. Figure 5 shows the maximum error in the predicted divergence of the radiative flux as a function of the Planck or reference temperature. It is observed that the sensitivity of the RC-FSK model to choice of Planck temperature is lower than the sensitivity of the FSCK II model to reference temperature. For the RC-FSK model, the standard deviations of Max Error are 0.4% and 0.87% for the CH_4-1atm and CH_4-4atm flames, respectively, whereas they are of 16.19% and 1.22% for the FSCK II model. This suggests that a look-up table for the RC-FSK model might be generated using a single, fixed Planck temperature without significant loss of accuracy. This would reduce both the size of the look-up table and the number of variables to interpolate, leading to a reduction in the computational time to retrieve the desired *k*-distributions.

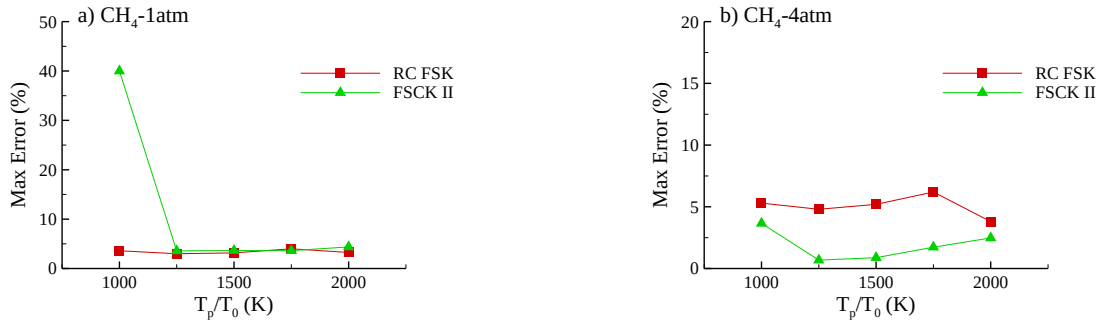

Figure 5. Effects of Planck (T_P) / reference (T_0) temperature on the maximum error on the divergence of the radiative flux. The abscissa axis uses T_P for the RC-SLW and T_0 for FSCK II. The errors for the radiative source term are based on the three radial profiles at z = 0.2, 0.4 and 0.6 m.

5. CONCLUSIONS

Radiative transfer predictions have been made using two versions of the full-spectrum correlated *k*-distribution model (FSCK and FSCK II), the Rank-Correlated full-spectrum *k*-distribution / Spectral-Line-Weighted-sum-of-gray-gases (RC-FSCK/RC-SLW) model, and a new version of the Weighted-Sum-of-Grey-Gases (WSGG) model. They are compared with the Narrow-Band CK (NBCK) model in four turbulent axisymmetric jet diffusion flames fueled either by hydrogen or methane at atmospheric and higher pressures with prescribed temperature fields. All spectral radiative property model parameters were generated using the same spectral absorption cross-section database. Model results suggest that the FSCK II method and the Rank-Correlated SLW/FSK model are the most mature gas radiative property models to be implemented in CFD codes, producing nominally the same accuracy. The FSCK model results in considerably higher error in the predicted radiative transfer. While the implementation of the WSGG model employed here reveals greater error than either the FSCK II or RC-FSK model predictions, its accuracy is satisfactory for engineering predictions in combustion situations. The FSCK II model is found to exhibit considerably greater sensitivity to the prescribed value of the reference temperature T_0 than the RC-FSK model's sensitivity to the Planck temperature T_P. The computation time for all of the gas radiative property models was documented and discussed.

REFERENCES

[1] M. F. Modest, D. C. Haworth, *Radiative Heat Transfer in Turbulent Combustion Systems: Theory and Applications,* Springer, 2016.

[2] M. K. Denison, B. W. Webb, "The spectral line-based weighted-sum-of-gray-gases model in non-isothermal non-homogeneous media", *ASME J. Heat Transfer*, vol. 117, pp. 359-365, 1995.

[3] M. F. Modest, H. Zhang, "The full-spectrum correlated-k distribution for thermal radiation from molecular gas-particulate mixtures", *ASME J. Heat Transfer*, vol. 124(1), pp. 30-38, 2002.

[4] F. André, R. Vaillon, “The spectral-line moment-based (SLMB) modeling of the wide band and global blackbody-weighted transmission function and cumulative distribution function of the absorption coefficient in uniform gaseous media”, *J. Quant. Spectr. Rad. Transfer*, vol. 109, pp. 2401–16, 2008.

[5] F. Cassol, R. Brittes, F.H.R. França, O.A. Ezekoye “Application of the weighted-sum-of-gray-gases model for media composed of arbitrary concentrations of H_2O, CO_2 and soot”, *Int. J. Heat Mass Transfer*, vol. 79, pp. 796–806, 2014.

[6] M. F. Modest, R. J. Riazzi, “Assembly full spectrum k-distribution from a narrow band database: effects of mixing gases, gases and non-gray absorpting particles and non-gray scatters in non-gray enclosures”, *J. Quant. Spectr. Radiat. Transfer*, vol. 90, pp. 169-189, 2005.

[7] V. P. Solovjov, B. Webb, “An efficient method for modeling radiative transfer in multicomponent gas mixtures with soot”, *J. Heat Transfer*, vol. 123, pp. 450-457, 2001.

[8] C. Wang, W. Geb, M. F. Modest, B. He, “A full-spectrum k-distribution look-up table for radiative transfer in nonhomogeneous gaseous media”, *J. Quant. Spectr. Rad. Transfer*, vol. 168, pp. 46-56, 2016.

[9] J. T. Pearson, B. W. Webb, V. P. Solovjov, J. Ma, “Updated correlation of the absorption line blackbody distribution function for H2O based on the HITEMP2010 database”, *J. Quant. Spectr. Rad. Transfer*, vol. 128, pp. 10-17, 2013.

[10] J. T. Pearson, B. W. Webb, V. P. Solovjov, J. Ma, “Effect of pressure on the absorption line blackbody distribution function and radiative transfer in H_2O, CO_2 and CO”, *J. Quant. Spectr. Rad. Transfer*, vol. 143, pp. 100-110, 2014.

[11] J. Cai, M. F. Modest, “Improved full-spectrum *k*-distribution implementation for inhomogeneous media using a narrow-band database”, *J. Quant. Spectr. Rad. Transfer*, vol. 141, pp. 65-72, 2014.

[12] F. André, V. P. Solovjov, D. Lemonnier, B. W. Webb, “Co-monotonic global spectral models of gas radiation in non-uniform media based on arbitrary probability measures: Theoretical foundations.”, *J. Appl. Math. Modeling*, vol. 50, pp. 741-754, 2017.

[13] V. P. Solovjov, F. Andre, D. Lemonnier, B. W. Webb, “The rank correlated SLW model of gas radiation in non-uniform media”. *J. Quant. Spectr. Rad. Transfer*, vol. 197, pp. 26-44, 2017.

[14] V. P. Solovjov , B. W. Webb , F. Andre, “The Rank Correlated FSK Model for Prediction of Gas Radiation in Non-Uniform Media, and its relationship to the Rank Correlated SLW Model”, *J. Quant. Spectr. Rad. Transfer*, vol. 214, pp. 120-32, 2018.

[15] F. André, F. Coelho, J.-L. Consalvi, F.H.R. Franca, M. Galtier, F. Nmira, V.P. Solovjov, B.W. Webb, « Accuracy of engineering methods for radiative transfer in CO2-H2O mixtures at high temperature”, in: Proceedings of the 9th International Symposium on Radiative Transfer (RAD-19), Eds. D. Lemonnier and B.W. Webb, Athens, Greece, 3-7 June 2019, Begell House, New York..

[16] F. André, "The ℓ-distribution method for modeling non-gray absorption in uniform and non-uniform gaseous media", *J. Quant. Spectr. Rad. Transfer*, vol. 179, pp. 19-32, 2016.

[17] F. André, "An analysis of symmetry issues in the ℓ-distribution method of gas radiation in non-uniform gaseous media", *J. Quant. Spectr. Rad. Transfer*, vol. 190, pp. 78-87, 2017.

[18] R. Demarco, J. L. Consalvi, A. Fuentes, S. Melis, "Assessment of radiative property models in non-gray sooting media", *Int. J. Thermal Sci.*, vol. 50, pp 1672-1684, 2011.

[19] H. Chu, J. L. Consalvi, M. Gu, F. Liu, "Calculations of radiative heat transfer in an axisymmetric jet diffusion flame at elevated pressures using different gas radiation models", *J. Quant. Spectr. Radi. Transfer*, vol. 197, pp. 12-25, 2017.

[20] J. Pearson, "The development of updated and improved SLW model parameters and its application to comprehensive combustion prediction", PhD dissertation, Brigham Young University, Provo, UT, 2013.

[21] H. Chang and T. Charalampopoulos, "Determination of the wavelength dependence of refractive indices of flame soot", *Proc. R. Soc.*, vol. 430, pp. 577-591, 1990.

[22] F. R. Centeno, R. Brittes, L. G.P. Rodrigues, F. R. Coelho, F. H. R. França, "Evaluation of the WSGG model against line-by-line calculation of thermal radiation in a non-gray sooting medium representing an axisymmetric laminar jet flame", *Int. J. Heat Mass Transf.*, vol. 124, pp. 475-483, 2018.

[23] F.R. Coelho, F.H.R. França. "WSGG correlations based on HITEMP2010 for gas mixtures of H_2O and CO_2 in high total pressure conditions," *Int. J. Heat Mass Transfer*, vol. 127, pp. 105-114, 2018.

[24] F. Nmira, J. L. Consalvi, F. André, "Pressure effects on radiative heat transfer in hydrogen/air turbulent diffusion flames", *J. Quant. Spectr. Rad. Transfwe*, vol. 220, pp. 172-179, 2018.

[25] J. L. Consalvi, F. Nmira F, D. Burot, "Simulations of sooting turbulent jet flames using a hybrid flamelet/stochastic Eulerian field method", *Combust. Theor. Model.*, vol. 20, pp. 221-257, 2016.

[26] L. Valiño, "A field Monte Carlo formulation for calculating the probability density function of a single scalar in a turbulent flow", *Flow. Turbul. Combust.*, vol. 29, pp. 2139-2146, 1998.

[27] M. P. Burke, M. Chaos, Y. Ju, F. L. Dryer, S. J. Klippenstein, "Comprehensive H_2/O_2 kinetic model for high-pressure combustion", *Int. J. of Chem. Kin.*, vol. 44, pp. 444-474, 2011.

[28] Z. Qin, V. V. Lissianski, H. Yang, W. C. Gardiner, S. G. Davis, and H. Wang, "Combustion chemistry of propane: a case study of detailed reaction mechanism optimization," *Proc. Combust. Inst.*, vol. 28, no. 2, pp. 1663–1669, 2000.

[29] P. R. Lindstedt, "Simplified Soot Nucleation and Surface Growth Steps for Non-Premixed Flames," in Soot Formation in Combustion, vol. 59, H. Bockhorn, Ed. Springer Berlin Heidelberg, 1994, pp. 417–441.

[30] E. H. Chui, G. D. Raithby, P. M. J. Hughes, “Prediction of radiative transfer in cylindrical enclosures with the finite volume method”, *J. Thermophys. Heat Transfer*, vol. 6, pp. 605-611, 1992.

[31] C. Wang, B. He, M. F. Modest, T. Ren, “Efficient full-spectrum correlated-k-distribution look-up table”, *J. Quant. Spectr. Rad. Transfer*, vol. 219, pp. 108-116, 2018.

[32] B.W. Webb, V.P. Solovjov, and F. André, “An Exploration of the Influence of Spectral Model Parameters on the Accuracy of the Rank Correlated SLW Model,” *J. Quant. Spectr. Rad. Transfer*, Vol. 218, 2018, pp. 161-170.

[33] J. Badger, B.W. Webb, and V.P. Solovjov, “An Exploration of Advanced SLW Modeling Approaches in Comprehensive Combustion Predictions,” *Comb. Sci. Tech.* (in press) https://doi.org/10.1080/00102202.2019.1678907.